Wind-Tunnel Investigation of the Separation Maneuver of Equal-Size Bodies

M. J. LANFRANCO*
Convair Division of General Dynamics, San Diego, Calif.

Two separation maneuvers, an abort and normal staging, were investigated experimentally for a configuration consisting of two equal-size, fully reusable, lifting-entry vehicles mounted in parallel. Three types of tests were performed for the situation of one body separating from the other; 1) single element, to provide basic single-body data 2) traverse, to provide interference data between the two bodies, and 3) captive trajectory, to simulate the actual separation maneuvers. The data indicates that for the abort maneuver, aerodynamic interference effects change the trim angle of attack without affecting stability and increase the normal and axial forces. Aerodynamic forces and moments alone are sufficient to allow recovery from the maneuver. For the normal staging maneuver, aerodynamic interference effects increase the stability of the body as well as the normal and axial forces.

Nomenclature

C_A = axial force coefficient
C_m = pitching moment coefficient
C_N = normal force coefficient
cg = center of gravity
g = acceleration due to gravity (32.2 ft/sec²)
L = length of the vehicle (ft)
M = Mach number
q = dynamic pressure (lb/ft²)
t = time (sec)
x,z = coordinate system fixed at cg of booster in the mate position (see Fig. 6)
α = angle of attack (deg)
δ_e = elevon deflection (deg) positive into the flow

Introduction

SPACE travel has led to a requirement for a transportation system that performs the duties of a shuttlecraft between Earth and an orbiting station. The necessity for low-operational cost has generated concepts for fully reusable vehicles consisting of lifting-body elements mounted in parallel (Fig. 1). All elements are rocket-powered, vertical-takeoff, horizontal-landing vehicles, with one element operating as an orbiter and the other(s) as a booster. At some point along the launch trajectory, the elements separate (Fig. 2).

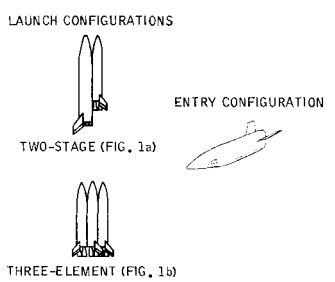

Fig. 1 Fully reusable launch vehicle configurations.

The separation of these bodies could introduce significant aerodynamic interference problems. For example, since a boost element is to be recoverable, it is important not only that the separation be clean but that the booster recovers from the separation maneuver.

This paper describes the results of an exploratory wind-tunnel investigation of separation maneuvers during normal staging and under abort conditions, using equal-size bodies originally derived from the three-element concept (Fig. 1b).

Captive Trajectory System

The captive-trajectory system[1] enables the trajectory of a body separating from another (stationary) body to be experimentally determined in a wind tunnel.

An analog computer combines force and moment data from a balance within the separating body with body dynamic characteristics information to compute the resultant trajectory. This trajectory is simulated by the six-degree-of-freedom support shown in Fig. 3.

The simulation includes the aerodynamic characteristics of the separating body during and just after separation as influenced by the flowfield generated by the stationary body, together with the mass properties and propulsion characteristics of the body itself. In this way, the effects of body release position and attitude can be studied.

The model support, an electromechanical positioning system with all axes of motion contained within a single mechanism, is independent of the stationary body. This mechanism has an envelope of motion lying within a cube about 30 in. on a side (Fig. 4). Drive motors, located in a case below the tunnel floor, are printed-armature electric motors with extremely fast response characteristics. A summary of the capabilities of the system is given in Table 1.

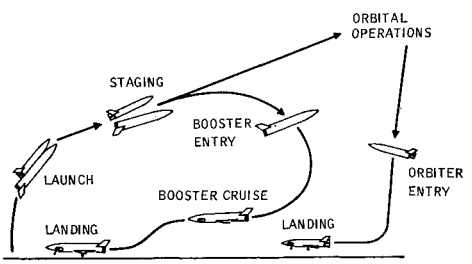

Fig. 2 Mission concept for fully reusable vehicle.

Presented as Paper 70-260 at the AIAA Advanced Space Transportation Meeting, Cocoa Beach, Fla., February 4–6, 1970; submitted February 26, 1970; revision received July 20, 1970.

* Senior Aerodynamics Engineer, Aerodynamics Section. Member AIAA.

Table 1 Captive trajectory mechanism capabilities

Item	Specification
Mach number range	0.5–4.0
Time scale	10:1–80:1
Time, drive motor—full stop to full speed	0.1 sec
Accuracy—maximum difference between command & actual velocity	±0.5% range
Maximum velocity	
Axial	2.4 in./sec.
Vertical	3.0 in./sec
Horizontal	5.2 in./sec
Pitch	20.7°/sec
Yaw	20.7°/sec
Roll	55.0°/sec
Range of movement	
Axial	28 in. (transonic) 36 in. (supersonic)
Vertical	30 in.
Horizontal	30 in.
Pitch	±45°
Yaw	±45°
Roll	±360°

The control system for the separating body model serves both as a positioning control and as an interface between the analog computer and the model support. Back-emf from the electrical drive motors is used as a feedback to the velocity control system. Two preselected set points are available: one is a "home" position for use during tunnel start and stop; the other is the "start" position or point of initial separation.

After the freestream flow has been established, the analog computer computes the trajectory using model strain-gage balance data in conjunction with body mass, moment of inertia, rocket thrust, altitude, and other data. This trajectory, transformed into velocity components, is then supplied to the support control drive motors, thus positioning the separating model in a smooth, accurate simulation of the separation trajectory. The analog program is time-scaled; thus, what is seen is an apparent slow-motion movement of the separating body through its separation trajectory. The balance outputs are converted to aerodynamic coefficients, and the actual position and angle outputs are processed into full-scale parameters.

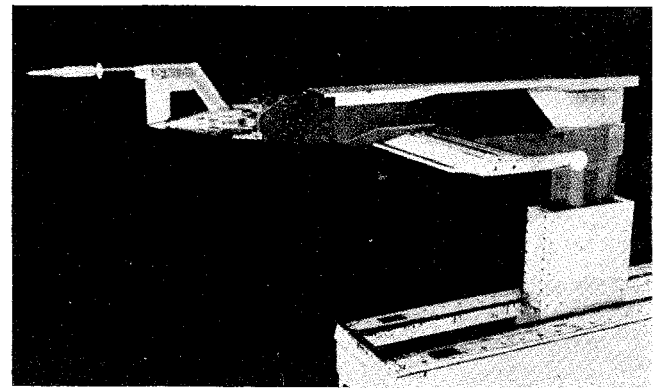

Fig. 3 Convair captive-trajectory mechanism.

Description of Models and Tests

The two steel models, representing the orbiter and booster, are $\frac{1}{194}$ scale replicas of two of the elements in the launch configuration (Fig. 1b). By making the assumption that the orbiter, using an active control system, is able to remain essentially undisturbed from its original trajectory, it was possible to support the orbiter from the tunnel wall with a fixed sting. The booster containing the balance was then sting-mounted to the captive-trajectory mechanism. Assembly and installation in the tunnel test section are shown in Fig. 5.

Three types of tests at two Mach numbers 1.63 and 4.0 were performed; 1)single element, 2) traverse, and 3) captive trajectory. The single-element test, i.e., the booster alone without the orbiter present, provided basic single-body data for determining incremental aerodynamic interference effects.

The traverse test provided aerodynamic interference data between orbiter and booster over a wide range of booster positions and orientations. In this test, the effects of the flowfield generated by the stationary orbiter on the aerodynamic characteristics of the booster were continuously recorded as the booster was traversed by the captive trajectory mechanism along the path shown in Fig. 6. Booster angle of attack was held constant for each traverse. This interference

Table 2 Data for full-scale simulation of trajectories

		Orbiter	Booster
Abort maneuver ($M = 1.63$)			
Weight	(lb)	485,397.0	294,301.0
Center of gravity[a]	(ft)	53.0, −0.5	58.5, −0.8
Moments of inertia	I_{XX}	429,000.0	280,000.0
(Slugs-ft²)	I_{YY}	10,020,000.0	8,030,000.0
	I_{ZZ}	10,000,000.0	8,000,000.0
	I_{XY}	0.0	0.0
	I_{YZ}	0.0	0.0
	I_{ZX}	25,200.0	59,000.0
Thrust (per nozzle)[b]	(lb)	382,000.0	382,000.0
Atmos. density (lb/ft³)		0.012282	0.012282
Staging maneuver ($M = 4.0$)			
Weight	(lb)	485,397.0	94,860.0
Center of gravity[a]	(ft)	53.0, −0.5	68.3, −2.6
Moments of inertia	I_{XX}	429,000.0	190,500.0
(Slugs-ft²)	I_{YY}	10,020,000.0	4,920,000.0
	I_{ZZ}	10,000,000.0	4,910,000.0
	I_{XY}	0.0	0.0
	I_{YZ}	0.0	0.0
	I_{ZX}	25,200.0	149,500.0
Thrust (per nozzle)[b]	(lb)	400,400.0	0.0
Atmos. density (lb/ft³)		0.00006669	0.00006669

[a] First number is X_{CG}, aft of nose; second is Z_{CG}; below reference waterline.
[b] Only one nozzle is operating. Two nozzles are operating on orbiter.

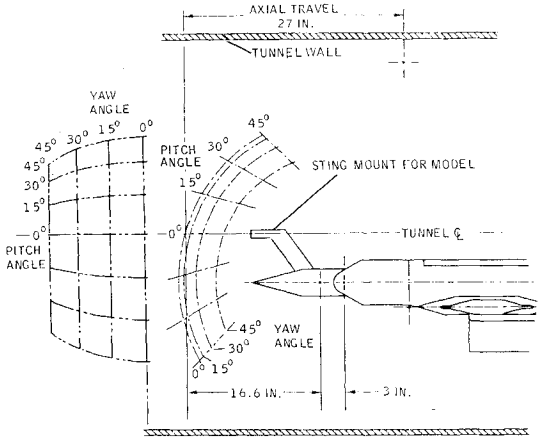

Fig. 4 Envelope of motion, captive-trajectory mechanism.

data will be used with semiempirical aerodynamic-characteristic prediction techniques to generalize the results to other configurations. Simulation of other trajectories via a dynamics computer program will also be possible with the interference aerodynamic forces.

Finally, the captive trajectory test simulated the actual abort and staging maneuvers to see if there were unanticipated problems to these maneuvers and also to evaluate various hinging and release mechanism schemes. Flight conditions simulated at abort: a) altitude, 49,000 ft, b) velocity, 1550 ft/sec, and c) dynamic pressure, 458 lb/ft^2; while at staging, a) altitude, 163,000 ft, b) velocity, 6,883 ft/sec, and c) dynamic pressure, 49.1 lb/ft^2.

Wind-tunnel Mach numbers were 1.63 and 4.0, respectively. Both vehicles were assumed to be in a gravity turn (free-fall), with the result that spatial orientation of the booster is given relative to the orbiter. The orbiter was assumed to have full thrust at separation. Plume effects caused by orbiter thrust were not simulated. Yaw and roll motions were prohibited (although forces and moments were measured), resulting in motion with only three degrees of freedom. The analog computer was preprogrammed with the data of Table 2 for the vehicles so that it could scale the booster motion to the full-size booster. In addition, values of the booster spatial coordinates and angular orientation relative to the orbiter, angular rates, and active control system variables were introduced into the computer prior to release from the point of initial separation. All controls were fixed at zero deflection.

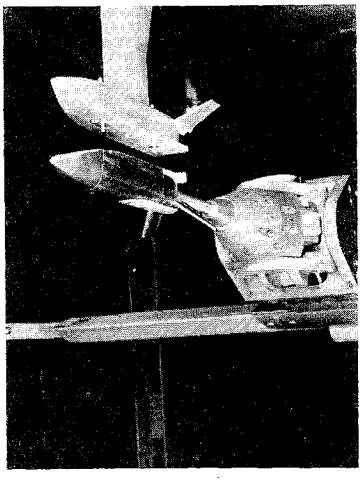

Fig. 5 Assembly and installation of captive-trajectory models in supersonic test section.

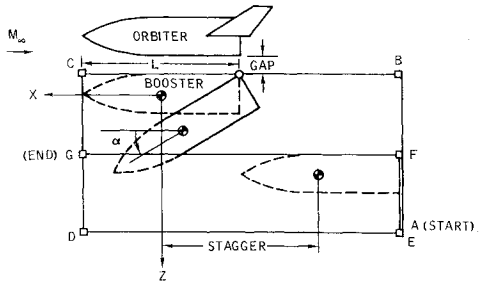

Fig. 6 Booster traverse path for M = 1.63, including coordinate system.

Schlieren movies were taken during all three types of tests to aid correlation of the data by the aerodynamic prediction techniques. Color movies were also taken during captive trajectory runs.

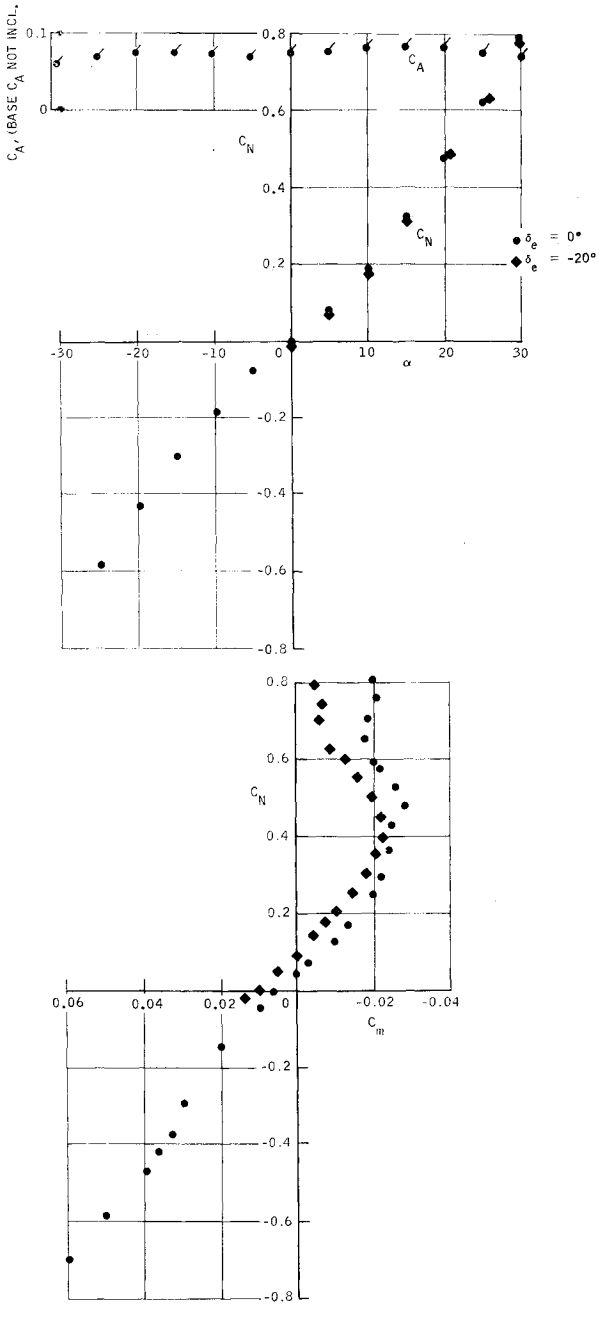

Fig. 7 Single element, 1/194 scale; longitudinal aerodynamic characteristics, body axis data, M = 1.63, R_e = 5.01 × 10^6.

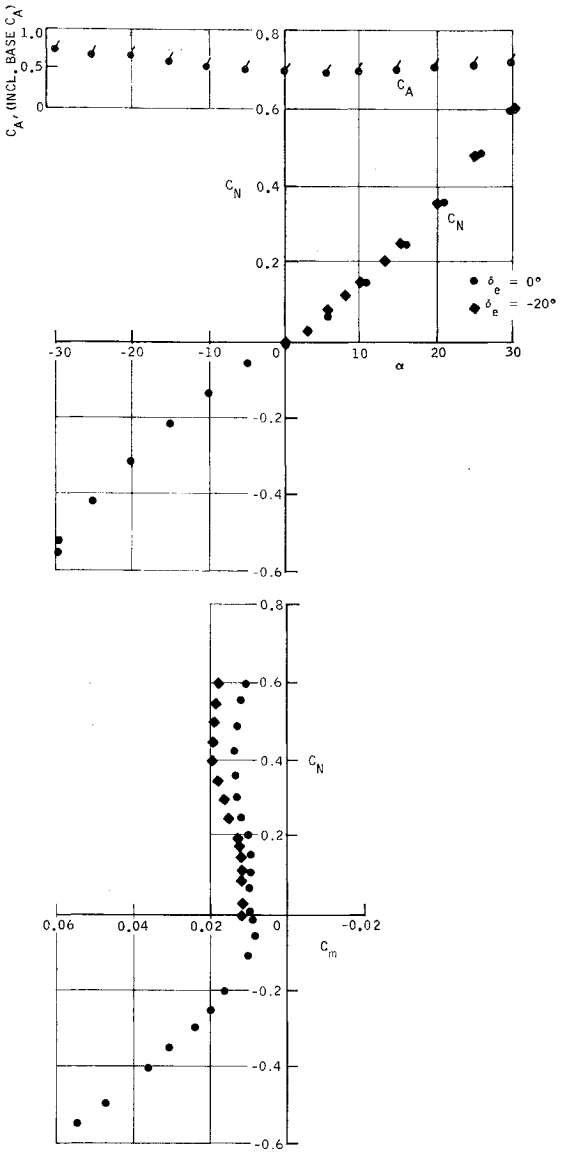

Fig. 8 Single element, 1/194 scale; longitudinal aerodynamic characteristics, body axis data, $M = 4.0$, $R_e = 9.69 \times 10^6$.

Data Presentation and Discussion

Longitudinal aerodynamic characteristics for the vehicle as a single element are presented in Figs. 7 and 8.

Reference conditions are shown in Table 3. At Mach 1.63, the vehicle is stable up to an attack angle of 20°, after which it becomes unstable. At Mach 4.0, however, the vehicle is stable at negative α, gradually becomes neutrally stable at small α, changes to unstable at $\alpha = 9°$, and is finally stable again to the maximum test angle of attack of 30°. The effect of a minus 20°-deflection (up out of the flow) of the elevons is also shown.

Sample data from the traverse test illustrating interference effects on the booster longitudinal characteristics as caused by the orbiter flowfield are shown in Figs. 9–12. (The

Table 3 Reference conditions

	Model	Full scale
Area, ft²	0.0619	2331.0
Length, ft	0.668	129.6
Moment center	0.524L aft of nose on reference waterline	

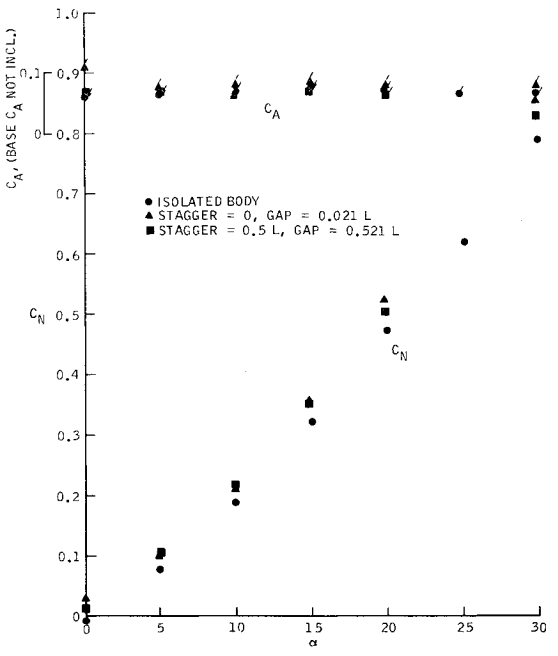

Fig. 9 Two-stage configuration, 1/194 scale; interference effects on longitudinal characteristics, traverse data, $M = 1.63$, $R_e = 5.01 \times 10^6$.

booster-orbiter configuration is shown in Fig. 5.) Increments in the forces over the single element (isolated body) data may be deduced from the figures as a function of angle of attack for the two chosen booster locations on the traverse path (Fig. 6). These increments are significant and are primarily due to the interaction of the orbiter bow shock with the booster surface. Of notable importance are the stability curves (Figs. 10 and 12). The interference effects at Mach 1.63 change the trim angle of attack without affecting stability. At Mach 4.0, the interference effects increase the stability of the booster at low angles of attack as well as changing the trim angle of attack.

Full-scale time histories of the booster's forces and moment for the configuration of Fig. 5 are presented in Figs. 13–15. At $M = 1.63$, note the change in the reference moment center

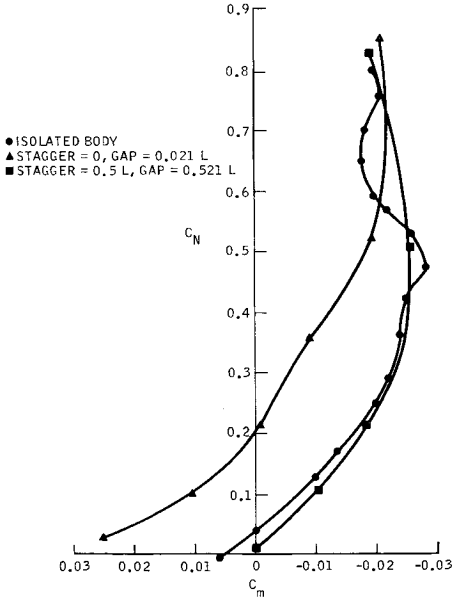

Fig. 10 Two-stage configuration, 1/194 scale; interference effects on longitudinal characteristics, traverse data, $M = 1.63$, $R_e = 5.01 \times 10^6$.

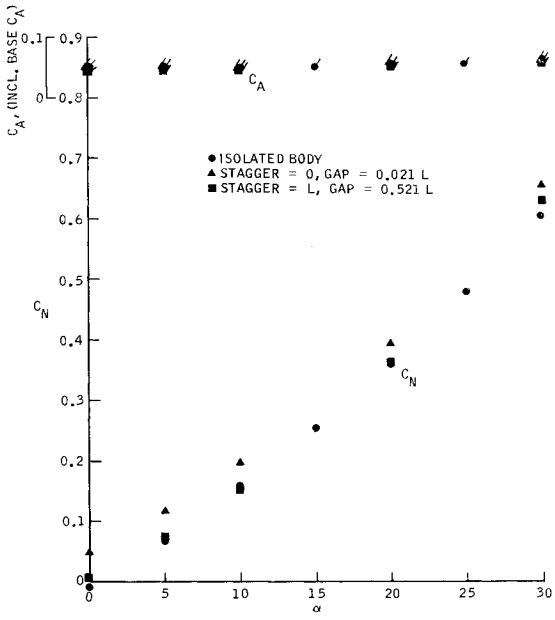

Fig. 11 Two-stage configuration, 1/194 scale; interference effects on longitudinal characteristics, traverse data, M = 4.0, R_e = 9.69 × 10⁶.

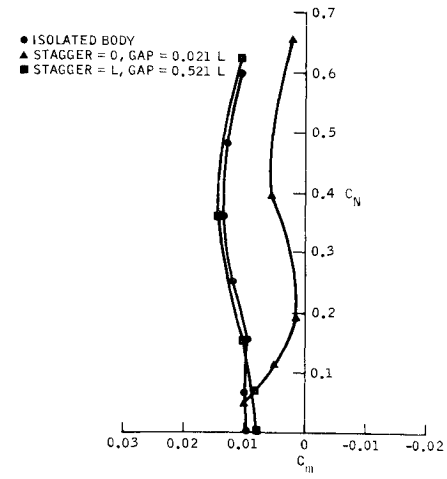

Fig. 13 Two-stage configuration, 1/194 scale; captive-trajectory time histories, no thrust on booster element, M = 1.63, R_e = 5.01 × 10⁶.

from the traverse data. Also shown is the variation of vehicle angle of attack with time as well as the location, full scale, of the booster cg with respect to the "mate" (stagger = 0, minimum gap) position shown in Fig. 6. The case presented in Fig. 13 at Mach 1.63 is the abort maneuver occurring at a dynamic pressure of 458 psf. The linkage system is a simple hinge at the aft end of the vehicle. The aerodynamic forces are used in performing the separation maneuver by allowing the booster to rotate about the hinge until it attains an angle of attack of 20°. The booster is then released with an initial pitch rate of 20°/sec. As can be seen from the variation of x, z, and α with time, the booster separates cleanly and recovers from the maneuver without requiring aerodynamic control forces or attitude control systems. Less than a $2g$ loading is exerted on the pilot from the effects of gravity and the angular acceleration about the cg. This angular acceleration is estimated from the product of the maximum value of $(d\alpha/dt)^2$ and the distance from the pilot to the vehicle cg. To increase confidence in the captive-trajectory system, a theoretical simulation of the separation maneuver was performed with the digital computer program of Ref. 2. Aerodynamic forces were provided for the program from the single-element and traverse tests. As is shown in Fig. 13, the correlation is quite acceptable.

The effects of a thrusting booster during the abort maneuver are shown in Fig. 14. Initial release angle and pitch rate are both zero. Only one engine is thrusting on the booster (through the cg), whereas all engines are thrusting on the orbiter. In this case the booster begins to rotate about its cg while still close to the orbiter, enhancing the possibility of collision between the two should unexpected disturbances

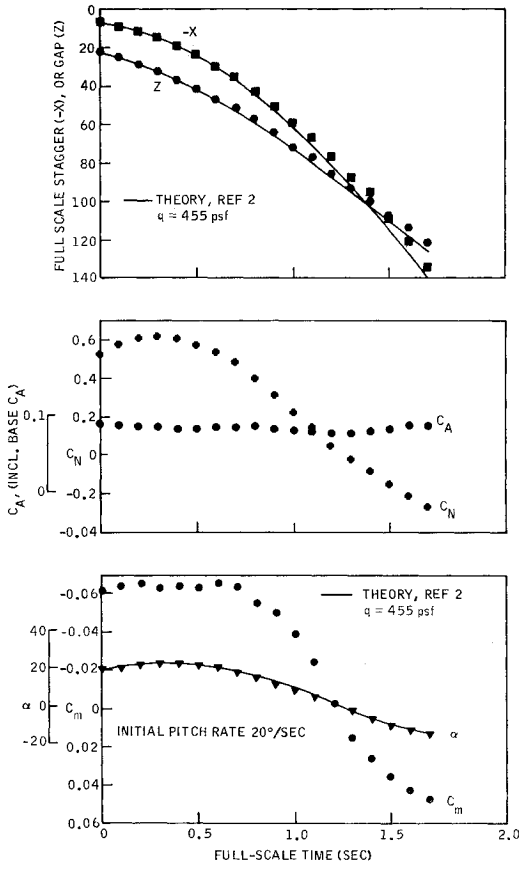

Fig. 12 Two-stage configuration, 1/194 scale; interference effects on longitudinal characteristics, traverse data, M = 4.0, R_e = 9.69 × 10⁶.

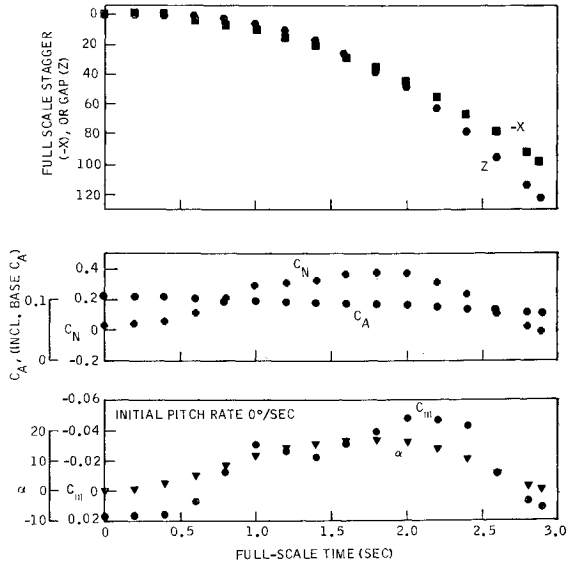

Fig. 14 Two-stage configuration, 1/194 scale; captive-trajectory time histories, thrust through c.g. of booster element, M = 1.63, R_e = 5.01 × 10⁶.

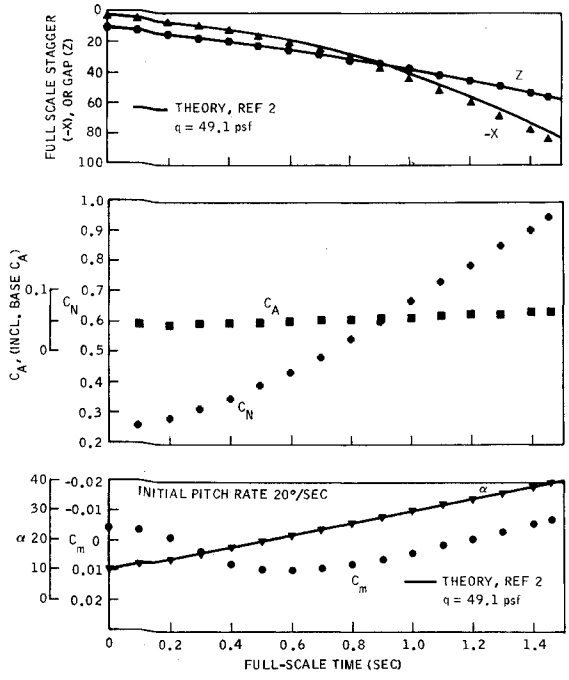

Fig. 15 Two-stage configuration, 1/194 scale; captive trajectory time histories, no thrust on booster element, $M = 4.0$, $R_e = 9.69 \times 10^6$.

occur. The booster finally separates, recovering from the maneuver without the necessity of active control input.

At Mach 4.0, the simulation of a normal staging maneuver, the effects of the aerodynamic forces are small since q is only 50 psf. This was verified by setting q equal to zero in the theoretical simulation of Ref. 2. Initial conditions for the maneuver are a release angle of 10° and a pitch rate of 20°/sec, with no thrust on the booster. The booster appears to separate cleanly (see Fig. 15), but the lack of aerodynamic forces and moments precludes recovery from the initial motion, at least in the time increment investigated. This is shown by α increasing monotonically with time. Recovery must then come from aerodynamic controls or attitude control systems. A comparison with the theoretical simulation of Ref. 2 again shows good agreement.

In a comparison between the traverse and the captive trajectory data, it was found that the value of C_m at $t = 0$ and $\alpha = 10°$ in Fig. 15 did not check with the corresponding value of C_m in Fig. 12. As of this writing, an acceptable explanation for the discrepancy is still to be found.

Finally, it is to be noted that all results and conclusions are highly configuration dependent.

Conclusions

At Mach 1.63 (abort maneuver):

1) The vehicle as a single element is aerodynamically stable in the α range of interest.

2) Aerodynamic interference effects are significant at small separation distances but do not change stability, although they do change the trim angle of attack and increase the normal and axial forces.

3) With no thrust on the booster, a clean separation is possible with a simple hinge release system and initial release angle and angular acceleration of 20° and 20°/sec, respectively. With booster thrust and initial values 0° and 0°/sec, a clean separation is not so certain.

4) Whether the booster is thrusting or not, aerodynamic forces and moments are sufficient to allow the booster to recover from the separation maneuver without active control input. The rate of recovery (no thrust case being the worst) is such that less than $2g$ loading is exerted on the pilot.

5) Good comparison between the theoretical simulation and the captive-trajectory results gives confidence to the captive-trajectory system.

At Mach 4.0 (normal staging maneuver)

1) The vehicle is not aerodynamically stable in the α range of interest for the reference cg chosen.

2) Aerodynamic interference effects increase the stability of the booster at low angles of attack as well as changing the trim angle of attack. Normal and axial forces are increased at small separation distances.

3) A simple hinge release system plus initial release angle and angular acceleration of 10° and 20°/sec will result in a clean separation for a nonthrusting booster.

4) The booster does not recover from the initial motions at release because of basic instability (Fig. 8) as well as the low-aerodynamic forces and moments. Aerodynamic controls or attitude control systems must be applied to allow recovery from the maneuver.

5) Good comparisons with the theoretical simulation gives confidence to the captive-trajectory system.

References

[1] Black, R. L., "High-Speed Store Separation—Correlation Between Wind-Tunnel and Flight-Test Data," *Journal of Aircraft*, Vol. 6, No. 1, Jan.–Feb. 1969, pp. 42–45.

[2] Hurley, M. J., "A Six-Degree, Multiple-Body Separation Simulation for Hinge and/or Linked Lifting-Entry-Vehicle Clusters," GDC-ERR-1377, Dec. 1969, Convair Division of General Dynamics, San Diego, Calif.